

**BANDWIDTH ENHANCEMENT OF PYRAMIDAL HORN
ANTENNA USING DIELECTRIC RESONATOR FEEDER**

ALI BIN OTHMAN

**UNIVERSITI SAINS MALAYSIA
2013**

**BANDWIDTH ENHANCEMENT OF PYRAMIDAL HORN
ANTENNA USING DIELECTRIC RESONATOR FEEDER**

by

ALI BIN OTHMAN

**Thesis submitted in fulfillment of the requirements
for the degree of
Doctor of Philosophy**

November 2013

ACKNOWLEDGEMENTS

I would like to express my appreciation by thanking those who have contributed in this dissertation. This dissertation would not have been possible without the help of many people, the foremost of these being the ALMIGHTY GOD, ALLAH S.W.T for giving me strength and courage. The next person that I would like to express my gratitude to is my supervisor, Associate Professor Dr. Mohd Fadzil Bin Ain for his ideas, advice, consultations and contributions throughout my dissertation. Despite his at times busy schedule, he was always available when I was in need of his scientific intuition and insights. I am most grateful to him for giving me the opportunity to work under his supervision and for offering me the moral and scientific support to achieve my academic goals. I would like to thank Professor Dr. Zainal Ariffin Bin Ahmad from Materials and Mineral Resources Engineering School for his invaluable scientific and moral support as my second supervisor.

I am greatly indebted to the administration and support staff of Engineering Campus for creating the ideal conditions for me in order to focus on my work. Special thanks go to Mr. Abdul Latip Hamid for his assistance and providing technical support in the Communications laboratory.

Thanks also go to Universiti Sains Malaysia (USM), Universiti Teknologi MARA (UiTM) and Ministry of Higher Education (MOHE) for providing the opportunity and supporting the research project. This research has been conducted under the contract USM RUT 1001/PELECT/854004. Last but not least, I would like to thank to my family and all my friends for their continuous encouragement and support.

TABLE OF CONTENTS

ACKNOWLEDGEMENTS	ii
LIST OF FIGURES	vii
LIST OF TABLES	xiv
LIST OF ABBREVIATIONS	xv
LIST OF SYMBOLS	xvii
ABSTRAK	xxii
ABSTRACT	xxiii
CHAPTER ONE	1
INTRODUCTION	1
1.1 Introduction	1
1.2 Motivation	1
1.3 Problem statements.....	2
1.4 Objectives of research	4
1.5 Research flow and limitations	4
1.6 Contributions	7
1.7 Thesis outline	8
CHAPTER TWO	10
REVIEW OF LITERATURE	10
2.1 Introduction	10
2.2 Pyramidal horn antenna.....	10
2.3 Coaxial probe to waveguide transition.....	14
2.4 Tuned coaxial probe to waveguide transition.....	17
2.5 Pyramidal horn antenna excitation methods.....	20
2.5.1 Pyramidal horn antenna excitation by a long thin crack	21
2.5.2 Pyramidal horn antenna excitation by stacked patch antenna.....	21
2.5.3 Pyramidal horn antenna excitation by Bow-tie and Vivaldi antenna.....	22
2.5.4 Pyramidal horn antenna excitation by microstrip antenna.....	23
2.5.5 Pyramidal horn antenna excitation by microstrip patch.....	24

2.6	Dielectric resonator antennas	25
2.7	Characteristics of DR	27
2.7.1	Dielectric constant.....	27
2.7.2	Quality-factor	28
2.7.3	Bandwidth	29
2.8	Cylindrical DRA.....	29
2.9	Annular sector DRA	32
2.10	Different coupling methods for DR.....	34
2.10.1	Coaxial probe	35
2.10.2	Microstrip transmission line/proximity coupling.....	36
2.10.3	Slot/aperture coupling	37
2.10.4	Co-planar slot loop coupling.....	38
2.10.5	Waveguide coupling.....	39
2.10.6	Conformal strip coupling	40
2.11	BW enhancement techniques	41
2.12	Summary	44
CHAPTER THREE.....		46
DESIGN PROCESS AND PARAMETER CHARACTERIZATION		46
3.1	Introduction	46
3.2	Computational electromagnetic.....	46
3.3	Pyramidal horn antenna design	47
3.4	Apex and phase center.....	58
3.5	Coaxial probe integrated pyramidal horn antenna, CPIPHA	62
3.5.1	CPIPHA return loss characteristic	65
3.5.2	CPIPHA radiation pattern	65
3.5.3	CPIPHA gain.....	68
3.5.4	CPIPHA input impedance	69
3.5.5	CPIPHA 3-D radiation pattern	70

3.6	Wideband hybrid DRA feeder design parameters.....	70
3.6.1	Modified structure of printed monopole antenna.....	71
3.6.2	Effect of truncated ground length, L_g	74
3.6.3	Effect of truncated ground width, W on modified structure	76
3.6.4	Radiation patterns of the modified structure.....	78
3.6.5	Printed monopole loaded with a DR	80
3.7	Summary	86
CHAPTER FOUR.....		87
RESULTS AND DISCUSSIONS		87
4.1	Introduction	87
4.2	Experimental characterization setup.....	87
4.3	Hybrid printed monopole DRA, HPMDRA (Design #1).....	90
4.3.1	Effect of a DR position with respect to the edge of the substrate.....	91
4.3.2	Parameter characterization	93
4.4	Hybrid rectangular printed monopole DRA, HRPMDRA (Design #2)	98
4.4.1	Parameter characterization	100
4.4.2	Parametric analysis.....	110
4.5	Hybrid DR integrated pyramidal horn antenna, HDRIPHA (Design #3) .	116
4.5.1	HDRIPHA excitation configuration.....	116
4.5.2	HDRIPHA parameter characterization	120
4.5.3	Parametric study on the impact of key parameters	132
4.6	Summary	142
CHAPTER FIVE.....		144
CONCLUSION AND RECOMMENDATION		144
5.1	Introduction	144
5.2	Conclusion.....	144
5.3	Recommendation.....	146
REFERENCES.....		148
LIST OF PUBLICATIONS		157

APPENDICES	158
Appendix-A Matlab code for pyramidal horn antenna design.....	158
Appendix-B Standard SMA flange mount jack with extended dielectric (Teflon)	173

LIST OF FIGURES

Figure No.	Title of Figure	Page
Figure 1.1 :	Flowchart illustrating the methodology of the research	6
Figure 2.1 :	Pyramidal horn and coordinate system: (a) pyramidal horn; (b) E-plane view; (c) H-plane view (Balanis, 2005)	13
Figure 2.2 :	Monopole antenna on infinite electric conductor	14
Figure 2.3 :	Calculated input reactance for monopole antenna as a function of antenna height, h (Stutzman and Thiele, 1998)	15
Figure 2.4 :	Coaxial transition with a SMA connector matching by d_x , H_p and S : (a) Side view; (b) Front view	16
Figure 2.5 :	Rectangular waveguide coaxial transition: (a) Inner geometry; (b) Equivalent circuit	18
Figure 2.6 :	Rectangular waveguide model of the transition	18
Figure 2.7 :	UWB pyramidal horn antenna excitation facility (Manoilov et al., 2007)	21
Figure 2.8 :	Configuration of a stacked patch pyramidal horn antenna (Shireen et al., 2008)	22
Figure 2.9 :	Pyramidal horn antenna fed by planar antennas (Pítra and Raida, 2010): (a) Bow-tie dipole; (b) Vivaldi	23
Figure 2.10 :	Integrated suspended square MSA fed pyramidal horn antenna (unit : cm) (Kumar et al., 2006)	24
Figure 2.11 :	Horn antenna excited by microstrip patch configuration (Ononchimeg et al., 2011)	25
Figure 2.12 :	Various DR geometries (Luk and Leung, 2003)	27
Figure 2.13 :	Cylindrical DRA geometry on metallic ground plane	29
Figure 2.14 :	Field distribution of the $TM_{01\delta}$ mode: (a) DRA field H_x and H_y at $z = 0$; (b) DRA fields E_y and E_z at $x = 0$ (Kajfez et al., 1984)	30
Figure 2.15 :	Field distribution of $HEM_{11\delta}$ mode: (a) DRA field H_x and H_y at $z = 0$; (b) DRA fields E_y and E_z at $x = 0$ (Kajfez et al., 1984)	31
Figure 2.16 :	Geometry of an annular sector DRA: (a) 3-D view; (b) Top and side views (Tam and Murch, 1999)	33

Figure 2.17 : Cylindrical DRAs: (a) Coupled through a microstrip line (Ain et al., 2007); (b) Coupled through a coaxial probe (De Young and Long, 2006); (c) Coupled through an aperture (Kwok-Wa et al., 1995)	35
Figure 2.18 : Cylindrical DRA with coaxial probe coupling (Leung et al., 1993)	36
Figure 2.19 : Cylindrical DRA with microstrip coupling (Ain et al., 2007)	37
Figure 2.20 : Cylindrical DRA with aperture coupling (Petosa, 2007b)	38
Figure 2.21 : Cylindrical DRA with co-planar slot loop coupling (Luk and Leung, 2003)	39
Figure 2.22 : Cylindrical DRA with waveguide coupling (Eshrah et al., 2005a)	40
Figure 2.23 : Configuration of the strip fed cylindrical DRA (Li and Leung, 2005)	40
Figure 3.1 : Pyramidal horn antenna dimensions and profile	50
Figure 3.2 : Waveguide port configuration	50
Figure 3.3 : Boundary conditions: (a) $\frac{1}{4}$ of the structure; (b) entire structure	51
Figure 3.4 : Simulated pyramidal horn antenna E-plane and H-plane radiation patterns at 14 GHz	52
Figure 3.5 : 3-D radiation pattern of pyramidal horn antenna in far-field at 14 GHz	53
Figure 3.6 : E- and H-plane patterns of pyramidal horn for constant P_e , P_h , W_a and different value of H_a	54
Figure 3.7 : E- and H-plane patterns of pyramidal horn for constants W_a , small H_a and different values of P_e , P_h	55
Figure 3.8 : E- and H-plane patterns of pyramidal horn for constants P_e , P_h , H_a and different values of W_a	55
Figure 3.9 : E- and H-plane patterns of pyramidal horn for constants H_a , small W_a and different values of P_e , P_h	56
Figure 3.10 : E- and H-plane patterns of pyramidal horn for constants, W_a , H_a and different values of P_e , P_h	57
Figure 3.11 : Return loss (S_{11}) of the pyramidal horn antenna obtained from CST MS ® simulations	57

Figure 3.12 : H-plane apex: (a) 3-D view; (b) side view	58
Figure 3.13 : E-plane apex: (a) 3-D view; (b) side view	60
Figure 3.14 : A simulated model of the transition	62
Figure 3.15 : Coaxial transitions with a SMA-connector depicts critical inner dimension of SMA flange mount jack ($D_p = 1.3$ mm, $\epsilon_r = 2.1$, Teflon diameter = 4.2 mm)	62
Figure 3.16 : CPIPHA geometrical configuration	64
Figure 3.17 : Return loss of CPIPHA	65
Figure 3.18 : CPIPHA radiation pattern	66
Figure 3.19 : Radiation patterns of CPIPHA configuration at 14.2 GHz	67
Figure 3.20 : CPIPHA gain	69
Figure 3.21 : Input impedance of CPIPHA	69
Figure 3.22 : 3-D Radiation pattern at resonant frequency at 14.2 GHz of the CPIPHA	70
Figure 3.23 : Geometry of printed strip microstrip transmission line	71
Figure 3.24 : Geometry of the modified printed monopole antenna	72
Figure 3.25 : Variation simulated return loss of the modified width printed monopole, W_2 with different monopole length of L_2	73
Figure 3.26 : Simulated resonant frequency variation of the modified width with printed monopole length of L_2	74
Figure 3.27 : Simulated effect of truncated ground length, L_g on resonant frequency of the modified printed monopole antenna	75
Figure 3.28 : Simulated BW variation with length of truncated ground plane, L_g of the modified structure	76
Figure 3.29 : Simulated return loss variation with the width of truncated ground plane W of the modified structure	77
Figure 3.30 : Simulated frequency variation with width of truncated ground plane, W	77
Figure 3.31 : Simulated BW variation with width of truncated ground plane, W	78

Figure 3.32 : Principal plane radiation patterns of the modified microstrip printed antenna at 10.3 GHz	79
Figure 3.33 : Variation of principal plane radiation patterns of the microstrip printed antenna at 10.3 GHz with length of truncated ground plane, L_g	80
Figure 3.34 : Variation of simulated return loss of printed monopole with different $50\ \Omega$ transformer length, L_1	81
Figure 3.35 : Simulated resonant frequency variation with the length of $50\ \Omega$ transformers, L_1	82
Figure 3.36 : Simulated BW variation with the length of $50\ \Omega$ transformers, L_1	82
Figure 3.37 : Simulated return loss of the printed monopole antenna alone and with DR loaded	84
Figure 3.38 : Simulated impedance BW of the printed monopole antenna alone and with DR loaded	85
Figure 3.39 : Magnitude of electric field distribution at the optimum position (HE_{118} mode at 16.38 GHz)	85
Figure 4.1 : Antenna measurement set-up and equipments facilities at the Faculty of Electrical Engineering, University Teknologi MARA Pulau Pinang	89
Figure 4.2 : Excitation geometry of HPMDRA feeder	91
Figure 4.3 : The optimized HPMDRA prototype: (a) front view; (b) back view	91
Figure 4.4 : Design HPMDRA in CST MS ® environment	92
Figure 4.5 : Structure of the HPMDRA: (a) side view; (b) front view; (c) back view	92
Figure 4.6 : Variation of simulated return loss with frequency for different values of displacement, d_y	93
Figure 4.7 : Variation of simulated return loss against frequency for different values of rotation angle, θ	94
Figure 4.8 : Simulated 3-D peak gain of the HPMDRA	94
Figure 4.9 : Radiation patterns at 12.08 and 16.38 GHz of the HPMDRA	95
Figure 4.10 : Co- and cross-polarization in H- and E planes at 12.08GHz	96

Figure 4.11: Co- and cross-polarization in H- and E planes at 16.38 GHz	96
Figure 4.12 : Input impedance of the HPMDRA	97
Figure 4.13 : Simulated surface current distribution at: (a) 12.08 GHz; (b) 16.38 GHz	98
Figure 4.14 : Geometry of the HRPMDRA: (a) side view; (b) front view; (c) back view	99
Figure 4.15 : Simulated return losses of the printed monopole antenna loaded with rectangular printed monopole	100
Figure 4.16 : Simulated return losses of the printed monopole antenna loaded with rectangular printed monopole and DR	101
Figure 4.17 : Variation of simulated return loss against frequency for different values of displacement, d_x of HRPMDRA	102
Figure 4.18 : Variation of simulated return loss against frequency for different values of displacement, d_y of HRPMDRA	102
Figure 4.19 : Simulated return loss of optimized HRPMDRA	103
Figure 4.20 : Simulated surface current distribution at: (a) 8 GHz; (b) 12.3 GHz; 16.2 GHz	104
Figure 4.21 : Simulated 3-D peak gain of the optimized HRPMDRA	105
Figure 4.22 : Principal plane radiation patterns of the HRPMDRA: (a) 8 GHz; (b) 12.3 GHz; (c) 16.2 GHz	106
Figure 4.23 : Simulated co- and cross-polarization in H- and E-planes at 8 GHz	107
Figure 4.24 : Simulated co- and cross-polarization in H- and E-planes at 12.3 GHz	107
Figure 4.25 : Simulated co- and cross-polarization in H- and E-planes at 16.2 GHz	108
Figure 4.26 : Simulated radiation pattern in E-plane and H-plane at 8, 12.3 and 16.2 GHz	109
Figure 4.27 : Plot of input impedance against frequency	109
Figure 4.28 : Variation of simulated return loss with Y_d	110
Figure 4.29 : Variation of simulated return loss with the rectangular patch length, n	111

Figure 4.30 : Variation of simulated return loss with the rectangular patch width, m	111
Figure 4.31 : Variation of simulated return loss with L_g	112
Figure 4.32 : Variation of simulated return loss with the dimension ground width W	113
Figure 4.33 : Variation of simulated return loss with thickness h of the used DR	113
Figure 4.34 : Variation of simulated return loss with the radius r_1 of DR at $r_2 = 0$	114
Figure 4.35 : Variation of simulated return loss with the radius r_2 of DR at $r_1 = 6$ mm	115
Figure 4.36 : Variation of simulated return loss with the offset feed, X_d	115
Figure 4.37 : Geometry of HDRIPHA excitation configuration	117
Figure 4.38 : Fabricated HDRIPHA: (a) Compact Hybrid DRA (i.e., HPMDRA); (b) Assembled Hybrid DRA; (c) Integrated pyramidal horn antenna	119
Figure 4.39 : Variation of simulated return loss with the displacement of d_y at $d_x = 0$ mm	120
Figure 4.40 : Variation of simulated return loss with the displacement of d_x at $d_y = 7$ mm	121
Figure 4.41 : Variation of simulated return loss with the rotation angle, θ at the displacement of $d_x = 0$ mm and $d_y = 7$ mm	121
Figure 4.42 : Measured and simulated return loss of the HDRIPHA	122
Figure 4.43 : Gain and the 3-D radiation patterns in linear scale	123
Figure 4.44 : Predicted gain of the HPMDRA (Design #1), HRPMDRA (Design #2) and HDRIPHA (Design #3)	125
Figure 4.45 : Simulated vertical and horizontal radiation pattern polarization of HDRIPHA: (a)10 GHz; (b)11 GHz; (c) 12 GHz; (d) 13 GHz; (e) 14 GHz; (f) 15 GHz; (g) 16 GHz; (h) 17 GHz; (i) 18 GHz	126
Figure 4.46 : Calculated radiation patterns of the hybrid DR integrated pyramidal horn antenna	127
Figure 4.47 : Calculated radiation patterns of the HDRIPHA at center frequency of 14 GHz	128

Figure 4.48 : 3-D Radiation pattern of the HDRIPHA at: (a) 10.60 GHz; (b) 12.00 GHz; (c) 15.38 GHz; (d) 16.46 GHz	129
Figure 4.49 : Contour plot of the E-field (V/m): (a) 10 GHz; (b) 14 GHz; (c) 18 GHz	129
Figure 4.50 : Surface current distribution of the HDRIPHA at different frequencies: (a) $f = 10.60$ GHz; (b) $f = 12.00$ GHz; (c) $f = 15.38$ GHz; (d) $f = 16.46$ GHz	131
Figure 4.51 : Plot of input impedance against frequency	132
Figure 4.52 : Simulated return loss of HPMDRA alone (Design #1) and combined with pyramidal horn (i.e., HDRIPHA of Design #3)	133
Figure 4.53 : Simulated effect of the ground plane length, L_g on the impedance BW of HDRIPHA	134
Figure 4.54 : Variation of simulated return loss curves for different values of the relative permittivity, ϵ_r of the used DR	135
Figure 4.55 : Variation of simulated return losses for different values of the inner radius, a of the used DR	136
Figure 4.56 : Variation of simulated return losses for different values of the outer radius, b of the used DR	136
Figure 4.57 : Variation of simulated return loss curves for different values of h of the used DR	137
Figure 4.58 : Variation of simulated return loss against frequency for different displacement of d_y values of HDRIPHA	138
Figure 4.59 : Variation of simulated return loss against frequency for different displacement of d_x values of HDRIPHA	138
Figure 4.60 : Simulated effect of the printed monopole length, L_2 on the impedance BW of HDRIPHA	139
Figure 4.61 : Simulated effect of the printed monopole width, W_2 on the impedance BW of HDRIPHA	140
Figure 4.62 : Simulated effect of the cavity back on the impedance BW of HDRIPHA	140
Figure 4.63 : Simulated effect of DR rotation angle on the impedance BW of HDRIPHA	141
Figure 4.64 : Simulated effect of the offset microstrip feed, X_d on the impedance BW of HDRIPHA	142

LIST OF TABLES

Figure No.	Title of Table	Page
Table 2.1 :	X'_{vp} values according to v and p values (Tam and Murch, 1999)	34
Table 2.2 :	Summary of measured DRAs with enhanced impedance BW	44
Table 3.1 :	Pyramidal horn antenna parameters at 14 GHz	49
Table 3.2 :	Apex and the phase center of a pyramidal horn	61
Table 3.3 :	Waveguide probe feed section dimensions	64
Table 3.4 :	Reflection characteristics and 3-dB HPBW of the CPIPHA	67
Table 3.5 :	Reflection characteristics and gain of the CPIPHA	68
Table 3.6 :	Constant parameters with different monopole length of L_2	72
Table 3.7 :	Constant parameters with different truncated ground length, L_g	75
Table 3.8 :	Constant parameters with different truncated ground plane width, W	76
Table 3.9 :	Constant parameters with different 50 Ω transformers length, L_1	81
Table 3.10 :	Dimensions of optimized parameters for the printed monopole antenna in mm	83
Table 4.1 :	Dimensions for the HPMDRA in mm	91
Table 4.2 :	Reflection characteristics and gain of the HPMDRA	95
Table 4.3 :	Reflection characteristic of the HPMDRA	97
Table 4.4 :	Optimized dimensions of parameters for HRPMDRA in mm	103
Table 4.5 :	Reflection characteristics and gain of the optimized HRPMDRA	106
Table 4.6 :	Simulated reflection characteristic of the HRPMDRA	108
Table 4.7 :	Simulated and measured reflection characteristic and gain of the HDRIPHA	124
Table 4.8 :	Simulated 3-dB beamwidth of HDRIPHA	127
Table 4.9 :	Comparison of simulated reflection characteristics and gain of the feeder designs	143

LIST OF ABBREVIATIONS

Abbreviation	Meaning
3-D	Three Dimension
AUT	Antenna Under Test
CPIPHA	Coaxial Probe Integrated Pyramidal Horn Antenna
CST MS ®	Computer Simulation Technology Microwave Studio ®
CPW	Coplanar Waveguide
CEM	Computational Electromagnetics
dB	Decibels
dB _i	dB Over Isotropic
DR	Dielectric Resonator
DRA	Dielectric Resonator Antenna
FIT	Finite Integrate Technique
GHz	Giga Hertz
HDRIPHA	Hybrid Dielectric Resonator Integrated Pyramidal Horn Antenna
HPBW	Half Power Beam Width
HP8720D	Hewlett Packard Network Analyzer
HPMDRA	Hybrid Printed Monopole DRA
HRPMDRA	Hybrid Rectangular Printed Monopole DRA
Ku-band	Kurtz-under Band
MATLAB ®	MATLAB Programming Software
PBA	Perfect Boundary Approximation
PC	Personal Computer
RF	Radio Frequency
RO4003	Hydrocarbon Ceramic Laminates

Abbreviation	Meaning
RT6010	RT/Duroid Ceramic Laminates
SMA	SubMiniature Version A
TEM	Transverse Electro Magnetic
UWB	Ultra Wideband
VNA	Vector Network Analyzer
VSWR	Voltage Standing Wave Ratio
WR62	Rectangular Waveguide Standard
WR90	Rectangular Waveguide Standard
XRD	X-ray Diffraction

LIST OF SYMBOLS

Symbol	Meaning
%	Percentage
α	Sector angle
f_1	1 st Resonant frequency
f_2	2 nd Resonant frequency
f_3	3 rd Resonant frequency
θ	Angle in degree
Ψ_e	Angle in the E-plane
Ψ_h	Angle in the H-plane
ω	Angular frequency
H_a	Aperture height
W_a	Aperture width
L_3	Apex length
ϕ	Azimuth angle
C	Capacitor
χ	Constant
π	Constant value (3.142)
ρ_1	Depth of the horn in the E-plane
ρ_e	Depth of the horn in the E-plane
ρ_2	Depth of the horn in the H-plane
ρ_h	Depth of the horn in the H-plane
G_o	Desired gain
ϵ	Dielectric constant

Symbol	Meaning
Δ_e	Different length in E-plane
Δ_h	Different length in H-plane
d_x	Displacement in x-axis
d_y	Displacement in y-axis
d	Distance/ Height of DR
ϵ_{eff}	Effective dielectric constant
P_e	E-plane flare length
J_y	Equivalent current density
M_x	Equivalent current density
L_f	Flare length
η	Free space impedance
μ_o	Free space permeability
ϵ_o	Free space permittivity
λ_o	Free space wavelength
λ_g	Guided wavelength
h	Height of DR/ Monopole height
P_h	H-plane flare length
L_1	H-plane side flare length
BW	Impedance BW
r_2	Inner radius
b	Inner radius of DR
S_{21}	Insertion loss
L_e	Length of E-plane apex

Symbol	Meaning
L_2	Length of flare
L_h	Length of H-plane apex
$\tan \delta$	Tangent loss
θ_m	Main lobe direction angle
V	Mode parameter
L_2	Monopole length
W_m	Monopole width
Q_e	Normalized Q-factor
dx	Off-center position
Y_d	Offset gap in y-axis
X_d	Offset gap in x-axis
Ω	Ohm
r_1	Outer radius
a	Outer radius of DR
X_p	Post normalized reactance
L_m	Printed monopole length
W_1	Printed monopole width
W_2	Printed monopole width
D_p	Probe diameter/Directivity of a pyramidal horn
H_p	Probe height
S	Probe position/Maximum acceptable VSWR
Q	Q-factor
r	Radius
X	Reactance/X-axis

Symbol	Meaning
n	Rectangular patch length
m	Rectangular patch width
T	Reference plane
®	Registered
ϵ_r	Relative dielectric permittivity
ϵ_{r1}	Relative dielectric permittivity of DR
ϵ_{r2}	Relative dielectric permittivity of substrate
R	Resistance
f_o	Resonant frequency
f_{res}	Resonant frequency
S_{11}	Return loss
X_{vp}	Root
β	Sector angle
c	Speed of light (3.0×10^8 m/s)
W_e	Stored energy
s	Stub
L	Substrate length
t	Thickness
W	Substrate width
E'_y	Tangential components of the E-field
H'_x	Tangential components of the H-field
P_{rad}	Total radiated power
L_g	Truncated ground plane length

Symbol	Meaning
k	Wave number
H_g	Waveguide height
Z_{WG}	Waveguide impedance
L_g	Waveguide length
W_g	Waveguide width
λ	Wavelength
W	Width
x'	x' -Axis
x	x -axis
y'	y' -Axis
Y	Y -Axis
y	y -axis
z'	z' -Axis
Z	Impedance/ Z -Axis
z	z -axis
X_a	Antenna Reactance
R_a	Antenna Resistance

PENINGKATAN LEBAR JALUR ANTENA TANDUK PIRAMID MENGUNAKAN PENYUAP PENYALUN DIELEKTRIK

ABSTRAK

Komunikasi satelit memainkan peranan penting dalam sistem telekomunikasi terkini. Justeru itu, antena berjalur lebar serta nilai gandaan yang tinggi menjadi sebahagian penyelesaian dalam mewujudkan konsep penggunaan frekuensi lebar. Antena tanduk piramid adalah yang terbanyak digunakan sebagai penyuar dalam sistem komunikasi satelit kerana kesesuaiannya dengan nilai gandaan serta aplikasi berjalur lebar yang tinggi. Umumnya, antena tanduk piramid dijana oleh peralihan suapan sepaksi, akan tetapi jalur lebar operasi peralihan suapan sepaksi adalah terbatas dan sering dianggap sebagai peralatan peralihan suapan yang berjalur lebar sempit. Tesis ini menerangkan teknik pembangunan serta analisa peningkatan jalur lebar antena tanduk piramid dengan menggunakan penyuar penyalun dielektrik (DR). Pada dasarnya antena penyalun dielektrik (DRA) adalah penyumbang utama kepada jalur lebar penyuar yang direka. Kesan gabungan dua penyalun menghasilkan pelbagai frekuensi dengan lebar jalur 48.15% pada -10 dB yang berpusat pada frekuensi 14.23 GHz manakala antena tanduk piramid dengan peralihan suapan sepaksi konvensional adalah 13.27%. Penyuar yang direka memberikan nilai gandaan purata 16.22 dBi dengan fleksibiliti galangan jalur lebar dan ciri radiasi yang bagus dalam operasi jalur lebarnya. Antena tanduk piramid meningkatkan nilai gandaan antena penyalun dielektrik (DRA) sebanyak 12.34 dBi. Keberkesanan reka bentuk penyuar yang dicadangkan telah menunjukkan potensi untuk mengeksploitasikannya dalam antena parabola bagi mengesan komunikasi satelit pada 10 hingga 18 GHz. Kesimpulannya kerja ini menawarkan alternatif kepada teknik konfigurasi penyuaran yang baru, cekap dan mudah untuk antena tanduk piramid.

BANDWIDTH ENHANCEMENT OF PYRAMIDAL HORN ANTENNA USING DIELECTRIC RESONATOR FEEDER

ABSTRACT

Nowadays, satellite communications play an important role in telecommunications. As a result, high gain and broadband antennas are part of the solution to establish a concept of wide frequency usage. Pyramidal horn antenna is most widely used as feed in satellite communication and tracking due to suitability for high gain and broadband applications. Generally, pyramidal horn antennas are fed by a coaxial feed transition. However, there is a fundamental limitation on the operating bandwidth (BW) of the coaxial feed transition and is often being considered as narrowband device. This thesis describes the development and analysis of the BW enhancement feeding technique for pyramidal horn antenna using a dielectric resonator (DR) feeder. The hybrid dielectric resonator antenna (DRA) found to be in essence contributing the BW of the design feeder. The combinational effect of two radiators produces multiple resonant frequencies and provides wideband 48.15% of measured -10 dB return loss impedance BW centered at 14.23 GHz, while that of the pyramidal horn with conventional coaxial feed transition is 13.27%. The designed feeder provide an average simulated gain of 16.22 dBi with flexibility in the impedance BW and the far-field radiation characteristics appears to be satisfied within the operating BW. The pyramidal horn improved the gain of the hybrid DRA by 12.34 dBi. The effectiveness of proposed design and preliminary results of the design have shown a potential to exploit the designed feeder to be used in a parabolic antenna for tracking of satellites applications at 10 to 18 GHz. In conclusion this work offers a new, efficient and relatively simple alternative feeding technique configuration for pyramidal horn antenna.

CHAPTER ONE

INTRODUCTION

1.1 Introduction

Pyramidal horn antenna is widely used for large radio astronomy, communication dishes, and satellite tracking. This is generally due to its simplicity in construction, high gain, ease of excitation, versatility, and preferred overall performance. Generally, pyramidal horn antennas are excited by a coaxial feed transition, which determine the BW and the polarization. However, the coaxial feed transition has relatively limited operating BW which cannot be used in wideband applications. In order to increase the frequency BW, several new excitation methods have emerged, and there is still much development possible. This introductory chapter presents the main reasons and motivation which contributed for the elaboration of the main subject of this thesis which is the development of a new feeding technique for pyramidal horn antenna using broadband hybrid DRA to be installed in a parabolic antenna for tracking of satellites applications at 10 to 18 GHz.

1.2 Motivation

The most important devices for satellite communications require broadband antenna to establish a concept of wide frequency usage (Coulibaly et al., 2006), and they function to receive, decode and convert the electromagnetic waves into electric current, or vice-versa. Dealing with space communications require a parabolic antenna which can communicate with satellites operating at certain frequency ranges for examples 10 to 18 GHz. Sometimes, some of these frequencies cannot be reached and a more complex system is needed. Broadband antenna feeds are part of the solution.

Although pyramidal horn have ease of excitation, which are simply fed either by rectangular, circular waveguides or by a coaxial feed (Balanis, 2005, Stutzman and Thiele, 1998), their frequency BW is limited. The feed waveguide providing a transition from coaxial to rectangular waveguides governs the BW and polarization of radiated wave. The operating BW and polarization are determined by a coaxial feed which acts as a quarter wavelength monopole antenna, and is backed by a quarter wavelength shorted section of the waveguide. Furthermore, the coaxial feed transition has limited operating BW and is often considered as a narrowband device. In order to provide greater BW for the feed network for pyramidal horn in satellite communications, wideband feeder should be developed. Therefore, new integrated feeding configurations of pyramidal horn antenna still need to be investigated. This work has been inspired by the need for simple construction, high gain, broadband operation (suitable for Ku-band application), higher efficiency and quality pyramidal horn antenna transition.

1.3 Problem statements

Numerous coaxial-to-waveguide probe transitions have been proposed over the years, nearly all of which have less than 35% of Radio Frequency (RF) BWs (Kooi et al., 2003). The experimental study in (Keam and Williamson, 1994) observed that by minor adjustment of the probe length and short-circuit distance, it was possible to obtain yet a greater BW from the transition. There are a number of requirements imposed on the operation of this component. Ideally, it should provide good power match between the two wave guiding systems and operate preferably over a large frequency range. Some modifications have been made to the probe regarding the enhancement of the impedance BW including by employing a dielectric coated

probe, a conducting disc attached to the end of the probe and a tuning sleeve adjacent to the probe. The design of most of these transitions is however empirical, and still challenging to enhance the impedance BW for specified low reflections (Ao et al., 2008, Hajian et al., 1995). Many types of these transitions are commercially available but most of them have been reported to be complex structure for integration with other circuits. In some applications, it is favorable to agitate a pyramidal horn with a printed-circuit structure. In this case, a transition between the coaxial cable and the printed-circuit transmission line can be eliminated, making it easy to integrate to horn with printed circuits. There have been some research results on pyramidal horn antennas excited by printed circuit structures such as the microstrip probe, dipole and patch antennas (Caillet et al., 2010, Methfessel and Schmidt, 2010a).

Hence, one of the challenges that are focused in this research is to investigate and design an efficient feeding configuration technique for pyramidal horn antenna, which can cover wide operational BW between 10 to 18 GHz band. One possible solution for achieving BW enhancement is by using a DRA to excite the pyramidal horn. DRAs are a practicable solution to obtain larger BWs due to its simplicity in design of any 3-D shape, whilst maintaining the size and similar radiation patterns. Furthermore, DRA has very small dissipation loss which can handle high power. The DRAs are attractive candidates for many types of applications due to their inherent merits of high radiation efficiency, wide BW, small size, low dissipation loss, and cost-effective applications. Moreover, they offer better design flexibility compared to the conventional antennas, which are considered unique characteristics rather than conventional metallic antennas. DRAs represent a good potential antenna technology for ultra-wideband communications since it is not limited to linear polarization.

1.4 Objectives of research

This thesis introduces the development of a new feeding technique for pyramidal horn antenna using hybrid DRA to be used in a parabolic antenna for tracking of satellite applications at 10 to 18 GHz. The main objective of this PhD research is to investigate the ability of utilizing a single DR with a combination of microstrip fed printed monopole. The proposed antenna shall be used to realize a new wideband and high gain integrated feeding configuration of pyramidal horn antenna. The specific objectives are outlined as follows:

1. To investigate, design, characterize the compact hybrid DRA with a combination of multiple radiators, microstrip fed printed monopole and DR in order to increase the operational BW.
2. To integrate the designed hybrid DRA into pyramidal horn antenna as a feeder, while still exhibiting the increased BW properties.
3. To measure the performance of a new integrated hybrid DRA feeding configuration for pyramidal horn antenna in terms of the BW and gain capabilities.

1.5 Research flow and limitations

A systematic approach was employed to achieve the research objectives of this thesis work. The research reported in this thesis is focused on the BW enhancement of pyramidal horn antenna using DR feeding technique. In the first part, two different compact hybrids DRA designs are proposed to show the BW enhancement properties. A combinational of multiple radiators technique was employed by using microstrip printed monopole and a DR. A printed monopole antenna is design to operate at the lower end of the desired frequency band, while the compact circular

sector DR is designed so that the DR resonant occurs at the upper end of the desired frequency band (i.e., 10 to 18 GHz). In the second part, only one of the designed hybrids DRA was used to excite the pyramidal horn antenna as a feeder. The target frequency band of the design is limited to the ranges that cover from 10 to 18 GHz. In the last part, the performance of the BW and gain were measured and compared. The objectives of the research have been accomplished by following the methodological procedures as illustrated in Figure 1.1:

- Theoretical study and review of the coaxial to rectangular waveguide transition and DRA structure were done to provide insight into DRAs. The mode structure of different geometries is studied including knowledge of the current state-of-the-art, as well as capabilities and limitations of different designs were understood. Particular attention is given to wide operational BW capabilities using a combination of multiple radiators technique, microstrip fed printed monopole and DR, as this is a turning point of this research.
- Simulations of the DRAs are carried out using a 3-D time domain finite integral technique power modeling software CST MS ® to increase the skill with the software and to evaluate whether the results obtained from the literature could be reproduced. Once the simulation method is satisfactory, investigations into designs that presented with wideband capabilities using CST MS ® is done to gain insight into what have been provided those key characteristics.
- New designs are then investigated, with the aim of providing a wideband capability. Once a design with the desired characteristics is found, the optimizations are carried out to obtain the optimum performances at the desired frequencies (i.e., 10 to 18 GHz).

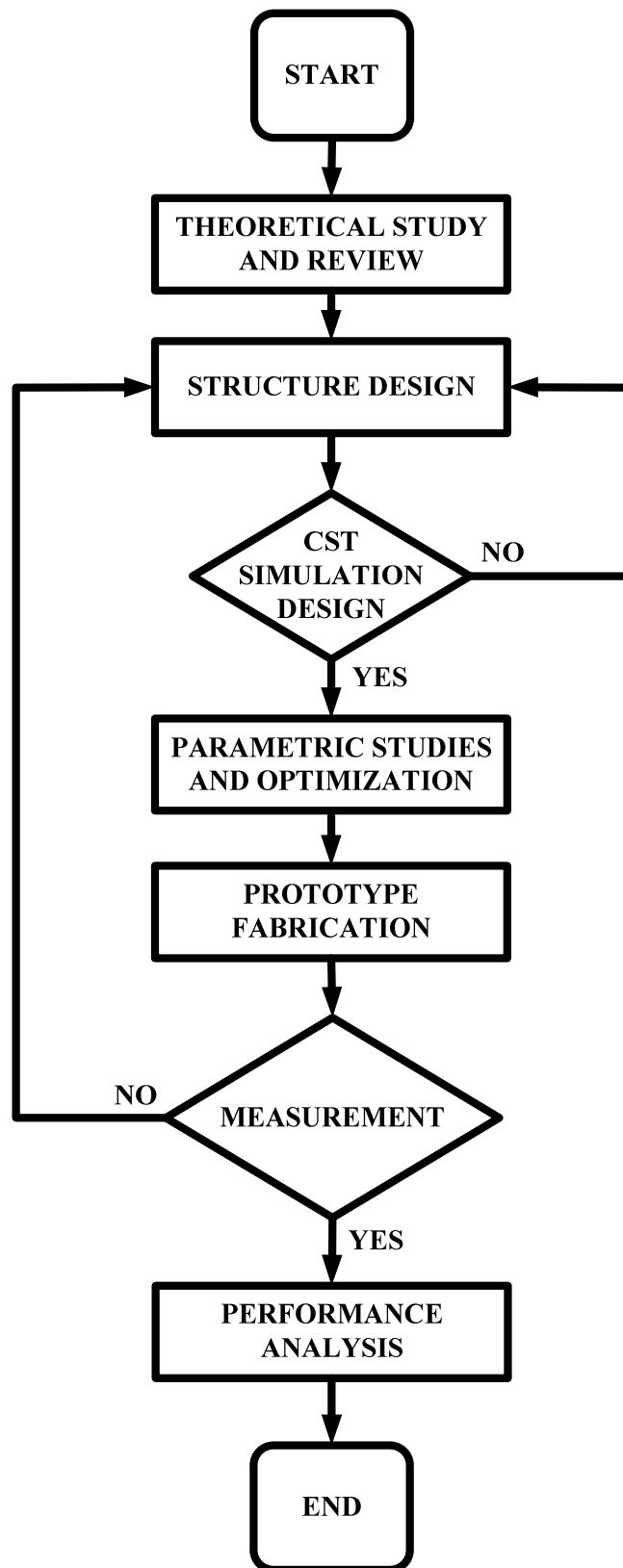


Figure 1.1 : Flowchart illustrating the methodology of the research

- Parametric studies are done to understand the repercussions of the designs variation and imperfection.
- Prototype of pyramidal horn antenna feeding configuration design is fabricated and measured to verify the accuracy of the concept.
- The results obtained for the prototype of pyramidal horn antenna feeding configuration are then compared with the current state-of-the-art of comparable probe type designs previously presented in literature.

1.6 Contributions

In this thesis, the pioneering idea of using hybrid DRA as a feeder for pyramidal horn antenna is demonstrated. To achieve this, a literature survey is done on the DRAs, including mode structures of basic geometries, coupling mechanisms, and state-of-the art designs. Also, different techniques to enhance the DRA's BW are found and individually analyzed, with the intent of producing wideband (over 10 to 18 GHz) frequency band. This led to new ideas and insight into the general field of DRA.

The complete work has three main contributions. First contribution is studying theoretical limitation on the BW of the coaxial feed transition and the BW enhancement technique using a DRA to excite the pyramidal horn.

The second contribution is the design and measurements of a DR feeding technique for pyramidal horn antenna with wideband and high gain capabilities. Two wideband feeder geometries hybrid printed monopole DRA (HPMDRA) and hybrid rectangular printed monopole DRA (HRPMDRA) were investigated for this particular design, both of which showed better performances compared to the state-of-the-art.

The third contribution is studying the ability to excite a pyramidal horn antenna with the designed hybrid DRA. The hybrid DRA consists of merging a multiple resonant bands of the DR and the feed network. A combination of multiple radiators, DR and microstrip fed printed monopole for the realization of wide operational BW capabilities to be used later in the feeding of 10 to 18 GHz band wave applications. The design presents the measured impedance match from 10.8 to 17.04 GHz (48.15%). The radiation characteristics are investigated between 10 to 18 GHz, and showed a boresight axis gain over 15 dBi over the entire frequency band with 10 dB beamwidths of $\pm 22^\circ$ in both E- and H-planes.

1.7 Thesis outline

The problem statement, research objectives, scope of research are presented in Chapter 1.

Chapter 2 presents the literature review on DRAs, and its usefulness on excitation of the pyramidal horn antenna. Theoretical presentations of DRAs are provided, which include the structural modes of basic geometries of DR, coupling mechanisms, and state-of-the art designs used to determine such parameters as Q-factor and resonant frequency. Reviews of few methods of enhancing impedance BW of DRAs were also presented.

Chapter 3 summarizes the results of modeling simulation that were run on prototype pyramidal horn designs using a 3-D power modeling software CST MS ®. The rationales behind the choice of the specific dimensions used in the prototype antennas were fully explained. Moreover, the simulated results were also presented indicating the effect of varying some design parameters.

Chapter 4 presents the experimental results for the fabricated prototype of pyramidal horn antenna feeding configuration. An analysis of parametric studies and summary of the obtained results were also presented.

Finally, Chapter 5 discusses the achievements of the thesis, and recommendation for future works based on limitation of the research.

CHAPTER TWO

REVIEW OF LITERATURE

2.1 Introduction

With the current trend in satellite communication technology, broadband antenna is a part of the solution to establish a concept of wide frequency usage. They are responsible for receiving, decoding and converting the electromagnetic waves into electric current, or vice-versa. Pyramidal horn antennas are used, in particular, due to their suitability for high gain and broadband applications. Generally, pyramidal horn antennas are excited by a coaxial feed transition. However, there is a fundamental limitation on the operating BW of the coaxial feed transition and often been considered as narrowband device. This chapter reviews of the pyramidal horn antenna, coaxial probe transition and DRAs. Also, a review of the previous research works on DRAs was introduced, in order to circumvent the BW limitation of the coaxial transition by implementing a new feeding technique using DRA to excite the pyramidal horn antenna.

2.2 Pyramidal horn antenna

As mentioned earlier in Chapter One, the horn antenna provides high gain, relatively wide BW, low voltage standing wave ratio (VSWR) with waveguide feeds, easy excitation and simple construction. Many different types of horn antennas exist, however, the pyramidal horn configuration serves as the primary horn antenna of interest. A pyramidal horn antenna combines the design of E- and H-plane sectoral horns. The tangential components of both fields, E- and H-fields, over the aperture of horn are approximated in (Rahmat-Samii et al., 1995) as:

$$E'_y(x', y') = E_o \cos\left(\frac{\pi}{W_a} x'\right) e^{-j[k(x'^2/\rho_2 + y'^2/\rho_1)/2]}$$

(2.1)

$$H'_x(x', y') = -\frac{E_o}{\eta} \cos\left(\frac{\pi}{W_a} x'\right) e^{-j[k(x'^2/\rho_2 + y'^2/\rho_1)/2]} \quad (2.2)$$

And equivalent current densities are given by:

$$J_y(x', y') = -\frac{E_o}{\eta} \cos\left(\frac{\pi}{W_a} x'\right) e^{-j[k(x'^2/\rho_2 + y'^2/\rho_1)/2]} \quad (2.3)$$

$$M_x(x', y') = E_o \cos\left(\frac{\pi}{W_a} x'\right) e^{-j[k(x'^2/\rho_2 + y'^2/\rho_1)/2]} \quad (2.4)$$

The pyramidal horns radiate field that correspond to a combination of both E- and H-plane of the horn antennas. The E-plane and H-plane patterns of the pyramidal horn antenna are identical to their respective sectoral counterparts. Detailed information is given by Balanis (Balanis, 2005) and Milligan (Milligan). To construct a pyramidal horn, the dimensions of P_e and P_h should be equal, such as in Figure 2.1 (Balanis, 2005):

$$p_e = (H_a - H_g) \left[\left(\frac{\rho_e}{H_a} \right)^2 - \frac{1}{4} \right]^{1/2} \quad (2.5)$$

$$p_h = (W_a - W_g) \left[\left(\frac{\rho_h}{W_a} \right)^2 - \frac{1}{4} \right]^{1/2} \quad (2.6)$$

where ρ_e and ρ_h are the depths of the horn in the E- and H-planes respectively, H_a and W_a are the length and width of the horn, while W_g and H_g represent the aperture length and width. The horn radiates most of its energy along the z-axis ($\theta = 0^\circ$). The directivity of a pyramidal horn can be determined from the following equation (Balanis, 2005):

$$D_p = \frac{\left(\frac{32}{\pi} \frac{H_a}{\lambda} \sqrt{\frac{50}{\rho_e / \lambda}} \right) \left(\frac{32}{\pi} \frac{W_a}{\lambda} \sqrt{\frac{50}{\rho_h / \lambda}} \right)}{10.1859 \sqrt{\frac{50}{\rho_e / \lambda}} \sqrt{\frac{50}{\rho_h / \lambda}}} \quad (2.7)$$

There are several possible goals for the design of a pyramidal horn. The aim can be for a horn to radiate a specified beamwidth, or a horn to radiate a specified gain, or an optimum-gain horn which attempts to produce the most efficient horn for a given size of aperture. Other parameters of interest to the design of pyramidal horns are the impedance and the phase center positions. The input impedance of most horns is generally well matched to the input waveguide, unless operation is near the cutoff frequency, or the flare angle is large so the mismatch at the waveguide-horn junction is significant (Olver, 1994).

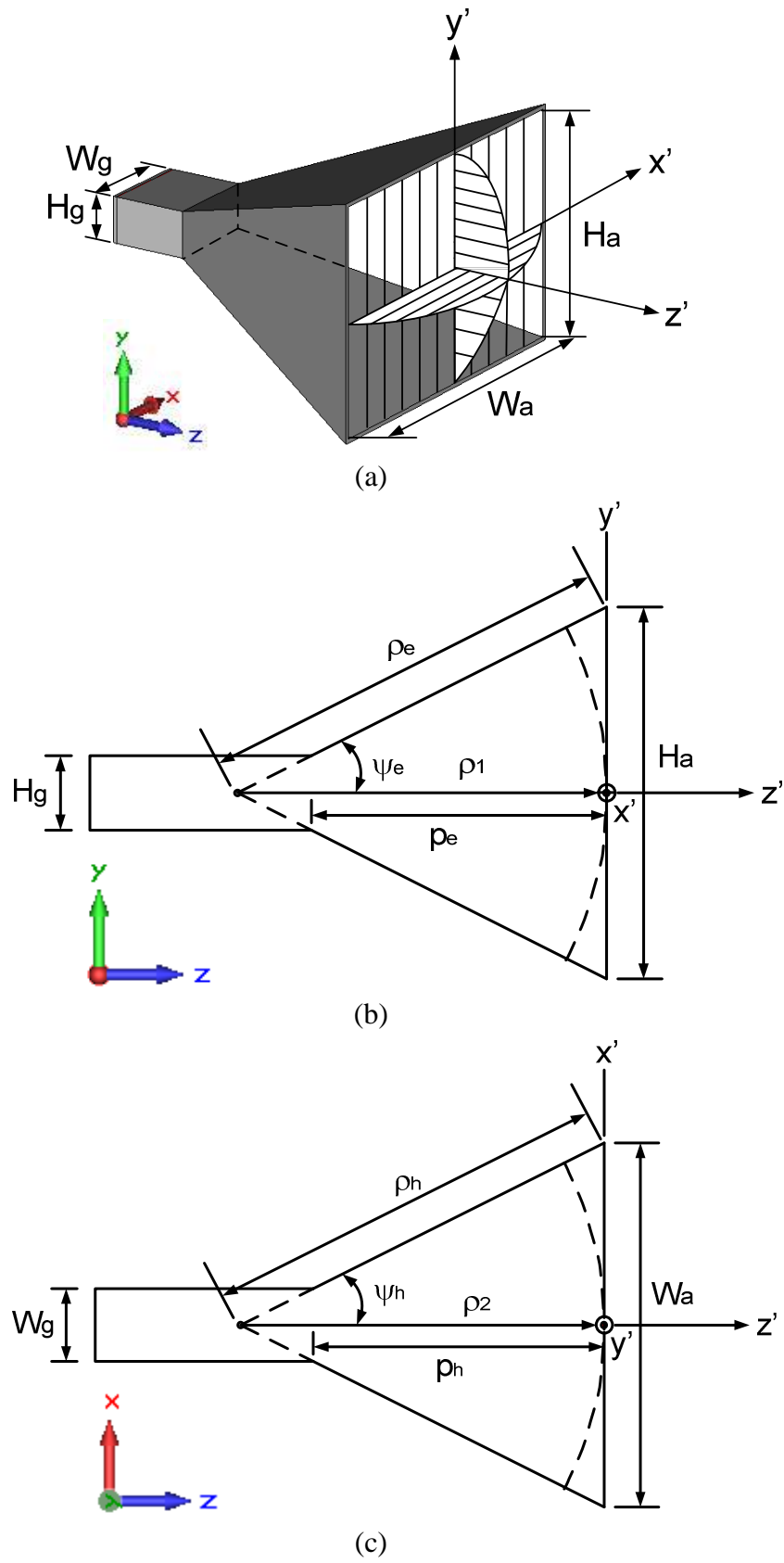


Figure 2.1 : Pyramidal horn and coordinate system: (a) pyramidal horn; (b) E-plane view; (c) H-plane view (Balanis, 2005)

2.3 Coaxial probe to waveguide transition

An elaborate discussion on the coaxial probe transition was given in (Collin et al., 1991). Initially, the coaxial probe transition is modeled with a monopole antenna over infinite lossless ground plane as illustrated in Figure 2.2.

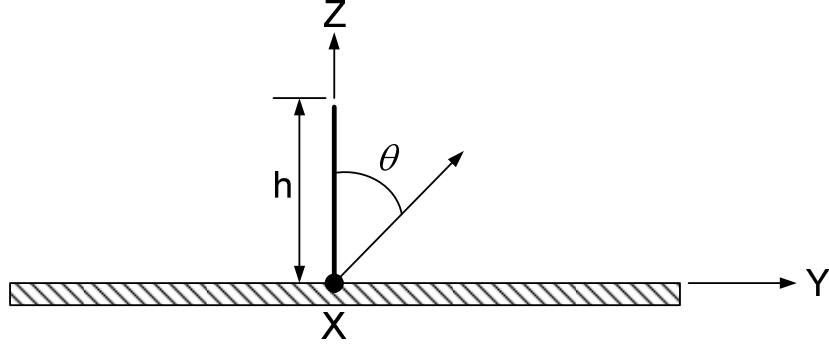


Figure 2.2 : Monopole antenna on infinite electric conductor

The total radiated power over the upper hemisphere of radius r can be written as (Collin et al., 1991):

$$P_{rad} = \oint W_{av} \cdot dS = \frac{1}{2\eta} \int_0^{2\pi} \int_0^{\pi/2} |E_\theta|^2 r^2 \sin\theta d\theta d\phi \quad (2.8)$$

where

$$E_\theta \cong j\eta \frac{kl_0 h e^{-jkr}}{4\pi r} \sin\theta \left[2 \cos\left(\frac{kh}{2\cos\theta}\right) \right] \quad z \geq 0 \quad (2.9)$$

$$E_\theta = 0 \quad z < 0 \quad (2.10)$$

and η and k are the free space impedance and wave number, respectively. Equation (2.9) can be used to plot $I_m(Z_{in})$ as a function of the monopole height, h . As shown in Figure 2.3, the most radiated power from the antenna can be achieved with $h = \lambda/4$ (Elliott, 2003). Therefore, $h = \lambda/4$ is the starting point for designing the conventional probe transition.

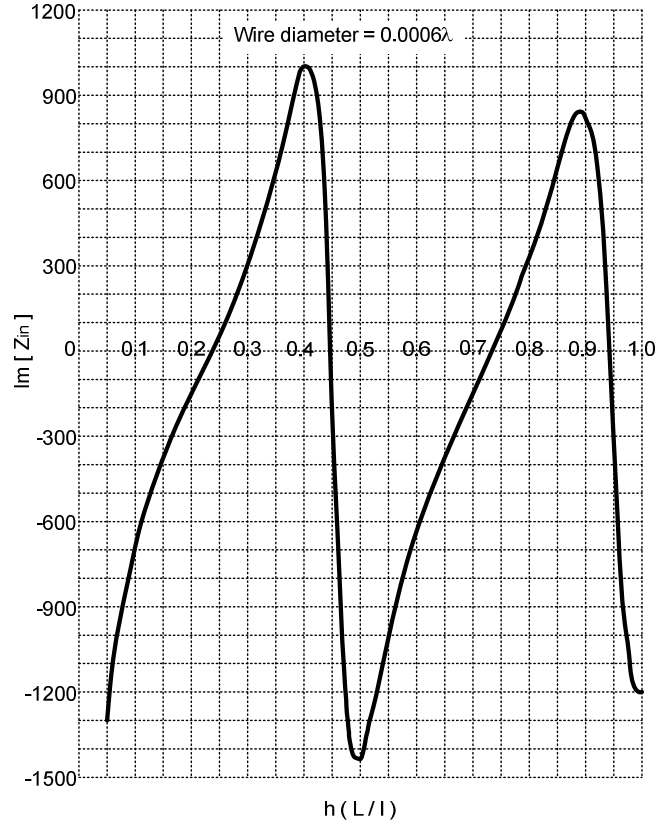


Figure 2.3 : Calculated input reactance for monopole antenna as a function of antenna height, h (Stutzman and Thiele, 1998)

Primarily, the electric and magnetic probes are two classic approaches that have been taken in designing coaxial line to waveguide transition. The major concerns of the design are finding the appropriate location to achieve an optimum impedance matching according to the waveguide walls, height and diameter of the probe. In a typical transition of coaxial to rectangular waveguides, coaxial feed

protrudes into the waveguide, which acts as a quarter wavelength ($\lambda/4$) monopole antenna, and is backed by a quarter wavelength ($\lambda/4$) shorted section of the waveguide.

An impedance match can usually be achieved by varying any two of the three dimensional parameters, the probe length (H_p), the off-center position of the probe (d_x), and the position in the waveguide (S). Figure 2.4 illustrates the monopole antenna probe made of a standard SMA flange mount jack connector and the parameters to be optimized to obtain an impedance match.

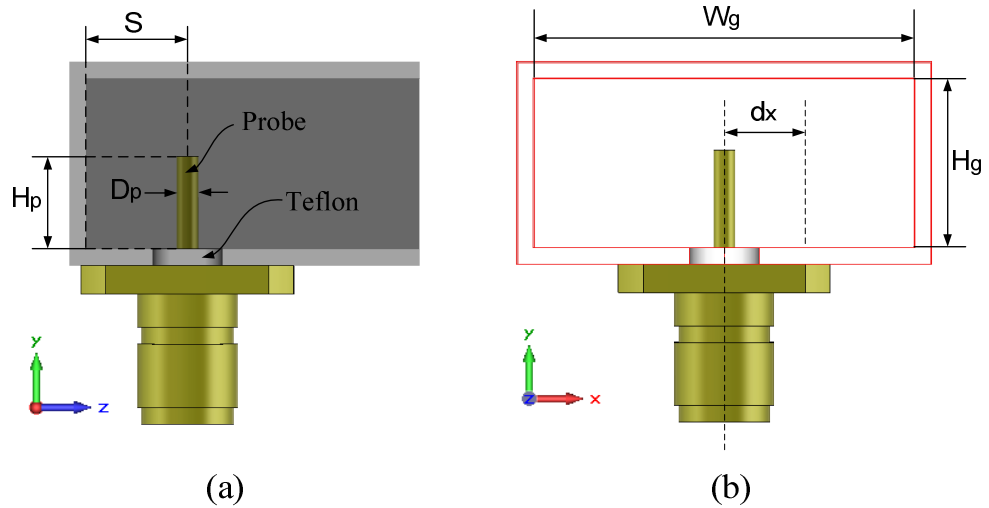


Figure 2.4 : Coaxial transition with a SMA connector matching by d_x , H_p and S : (a) Side view; (b) Front view

Some modifications have been made to the probe regarding the enhancement of the impedance BW. For instance, by employing probe coated with dielectric material, a tuning sleeve is placed adjacent to the probe and adding a conducting disc-ended probe. The designs of these transitions are yet empirical and still challenging to enhance the impedance BW for the low reflections (Ao et al., 2008, Hajian et al., 1995). The analysis of this type of transition has gained immense attention from numerous researchers (Williamson, 1985, Jarem, 1991, Bialkowski,

1991). A good quality coaxial-to-waveguide transition of a solid, straight, hollow probe and a sleeve transition was analyzed and reported in (Williamson, 1985), (Jarem, 1991) and (Bialkowski, 1991). However, the aim was not at wideband transition. In (Bialkowski, 1991) and (Bialkowski, 1995), the transition incorporating a probe with dielectric coated including a disc-ended probe are considered. The VSWR of greater than 1.3 over the whole X-band were obtained. Many types of these transitions are commercially available, though most of them have been reported to exhibit complex structures for integration with other circuits.

2.4 Tuned coaxial probe to waveguide transition

Due to the wide difference in impedances of a coaxial line and waveguide of this type of transition, matching can be obtained by combining suitable series and parallel reactances. This transition consists of a coaxial feed which acts as a quarter wavelength monopole antenna inside, and is backed by a quarter wavelength shorted section of the waveguide. The tuning can be achieved by varying the inner conductor of a coaxial and the use of a shorted waveguide stub. The inner geometry and equivalent circuit of typical coaxial transition are illustrated in Figures 2.5(a) and (b), where the reference plane T is split between the waveguide and the coaxial. The equivalent impedance of the waveguide is represented by a resistor. The transition is represented by a series capacitive reactance with the coaxial line, while the equivalent waveguide susceptance stub is represented by a shunted waveguide.

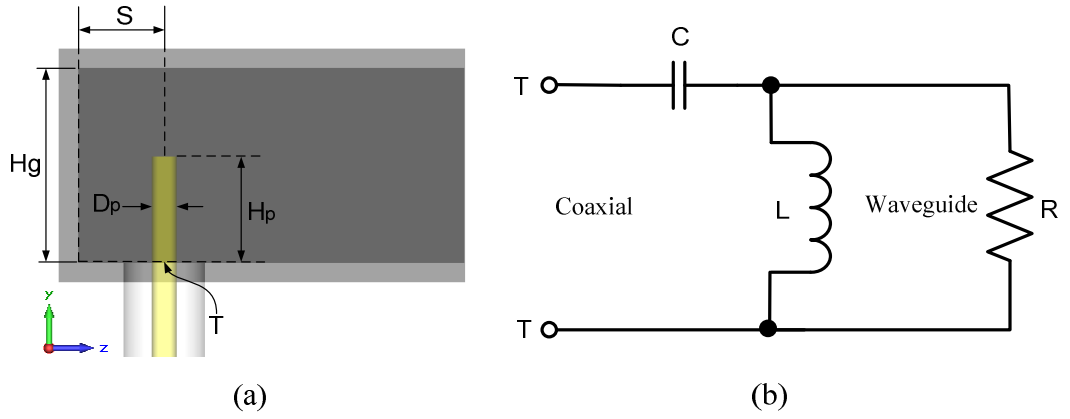


Figure 2.5 : Rectangular waveguide coaxial transition: (a) Inner geometry; (b) Equivalent circuit

The location, S from the closed end of the waveguide causes the signal from the probe to be reflected from the closed end back toward the open end of the waveguide as shown in Figure 2.6. H_p acts as a $\lambda/4$ vertical monopole antenna, and it sets up vertically polarized electromagnetic wave in the waveguide. Over $\lambda/4$ distance, the reflected signal appears back at the probe in phase to aid the signal going in the opposite direction.

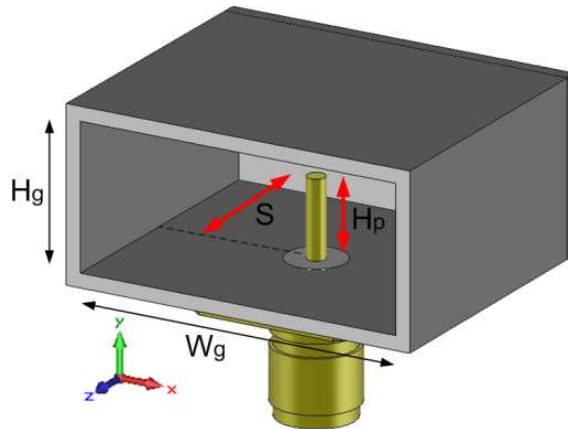


Figure 2.6 : Rectangular waveguide model of the transition

As shown in Figure 2.5, gives the input impedance according to (Delmotte, 2001) is given by:

$$Z_i = R + jX \quad (2.11)$$

where

$$R = \frac{Z_o}{2\pi^2} \frac{\lambda\lambda_g}{W_g H_g} \sin^2\left(\frac{2\pi S}{\lambda_g}\right) \tan^2\left(\frac{\pi H_p}{\lambda}\right) \quad (2.12)$$

$$X = \frac{Z_o}{4\pi^2} \frac{\lambda\lambda_g}{W_g H_g} \tan^2\left(\frac{\pi H_p}{\lambda}\right) \left[2X_p + \sin\left(\frac{4\pi S}{\lambda_g}\right) \right] \quad (2.13)$$

with

$$Z_o = \sqrt{\mu_o \epsilon_o} = 120\pi \Omega \quad (2.14)$$

and X_p represents the post normalized reactance with respect to the waveguide. It can be seen that the input impedance can be equalized to the coaxial line impedance by varying H_p and S since X_p is a function of H_p . For matching, the input X should be equal to zero ($X = 0$), and from Equation (2.13) gives the following expression results:

$$2X_p = -\sin\left(\frac{4\pi S}{\lambda_g}\right) \quad (2.15)$$

and

$$|X_p| \leq \frac{1}{2} \quad (2.16)$$

Thus, X_p is near resonant condition $X_p = 0$. Typically the height H_p is in the order of equal to $\lambda/4$ at resonant. Note that the equations are applicable if H_p is significantly less than H_g . If H_g is less than $\lambda/4$, the capacitance action between the tip of the H_p and the waveguide wall determines the resonant. In this condition, the tuning is vitally reliant on $(H_g - H_p)$ and the correct profile of the H_p tip. The following is the X_p expression given by Collin (Collin et al., 1991):

$$X_p = \frac{W_g}{2\lambda_g} \left\{ \ln \frac{2W_g}{\pi \left(\frac{D_p}{2} \right)} + \frac{0.0518k_0^2 W_g^2}{\pi^2} - 2 \left(1 - \frac{D_p}{W_g} \right) - 2k_0^2 \sum_{m=1}^{\infty} \left[1 - \frac{\sin^2 \left(\frac{m\pi H_p}{2H_g} \right)}{\sin^2 \left(\frac{k_0 H_p}{2} \right)} \right]^2 \frac{K_0 \left(k_m \frac{D_p}{2} \right)}{k_m^2} \right\} \quad (2.17)$$

where

$$k_m^2 = \left(\frac{m\pi}{H_g} \right)^2 - k_0^2 \quad (2.18)$$

2.5 Pyramidal horn antenna excitation methods

Pyramidal horn antenna has been traditionally realized by feeding the input waveguide with coaxial probe transition. The usage of coaxial feed transition is very common for low and medium power pyramidal horn antennas. However, there is a fundamental limitation on the operating BW of the coaxial feed transition. In some applications, it is favorable to excite a pyramidal horn with a printed-circuit structure. In such case, a transition between the coaxial cable and the printed-circuit transmission line can be eliminated, making it easy to integrate to horn with printed circuits. There have been some research results on pyramidal horn antennas excited by printed circuit structures such as the microstrip probe, dipole and patch antennas (Methfessel and Schmidt, 2010b, Caillet et al., 2010).

2.5.1 Pyramidal horn antenna excitation by a long thin crack

A study on the method of pyramidal horn excitation by a crack is proposed by (Manoilov et al., 2007). The pyramidal horn antenna working in ultra-wideband (UWB) frequency range of 1 GHz to 18 GHz is given as a basic one. As it can be seen in Figure 2.7, the coaxial line is disposed in the middle of the horn back, which parallel to the wide wall is employed for the excitation. The connection from the coaxial line to the H-shaped waveguide is carried out by the long thin crack along a coaxial line formative. The complete power transmission is realized by the longitudinal dielectric insertion from the coaxial line to a long crack. It is reported that the performance shows maximal VSWR about 2.6. The method provide reasonably good characteristics however, it require complex transition.

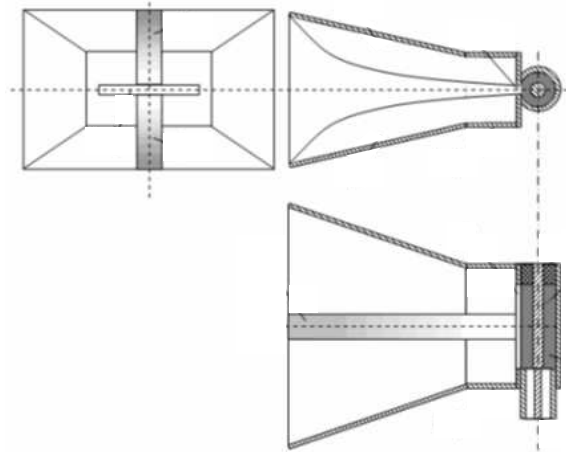


Figure 2.7 : UWB pyramidal horn antenna excitation facility (Manoilov et al., 2007)

2.5.2 Pyramidal horn antenna excitation by stacked patch antenna

An alternative method has been reported by (Shireen et al., 2008). The paper presents high gain and wide BW horn antenna excited by stacked patch antenna with 30% BW is achieved centered at 94 GHz. Several transitions of the coplanar waveguide (CPW) were reported in the past. However, all of them required truncation of the

planar circuit where these transitions are not suitable for antenna array configuration from the fabrication and integration points of view. Shireen et al. (Shireen et al., 2008) proposed a novel transition from CPW to horn antenna for integration with millimeter wave or optical receiver circuit. The method of the excitation is based on the slot coupling and stacked patch antenna technique for BW enhancement. The excitation method is depicted in Figure 2.8, showing the configuration of a CPW fed stacked patch with a pyramidal horn.

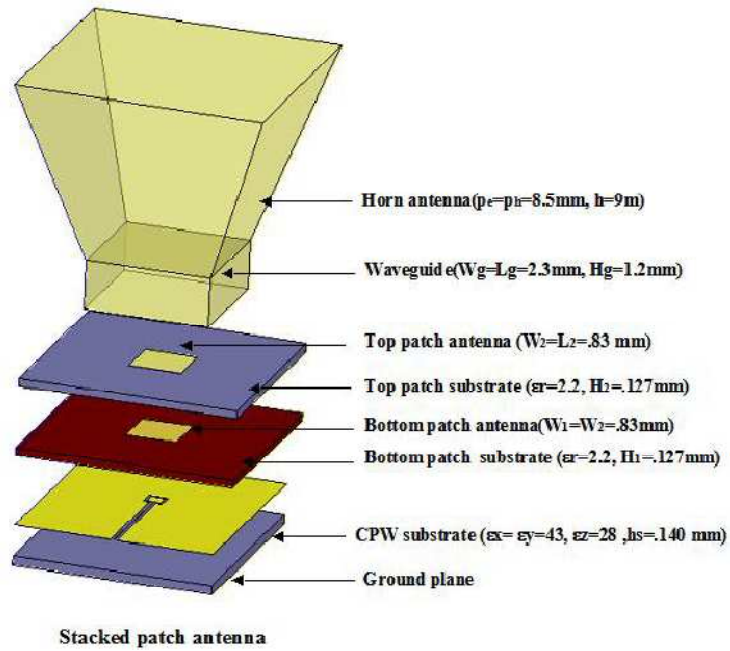


Figure 2.8 : Configuration of a stacked patch pyramidal horn antenna (Shireen et al., 2008)

2.5.3 Pyramidal horn antenna excitation by Bow-tie and Vivaldi antenna

A simple method of excitation is reported by directly placing the planar antenna on the pyramidal horn as illustrated in Figure 2.9 (Pítra and Raida, 2010). The result shows that the horn maintains the impedance BW of the planar horn feeder (i.e., Bow-tie and Vivaldi antennas). Both Bow-tie dipole and Vivaldi slot antennas

achieve wide BW of 18.49 GHz and 24.7 GHz respectively when they are placed inside the horn. Besides that, it is found that the gains of both antennas increase four times higher compared to standalone structure. Pyramidal horn antenna excited with wideband planar antennas provides reasonably good characteristics but the discussion on the impedance matching is not given.

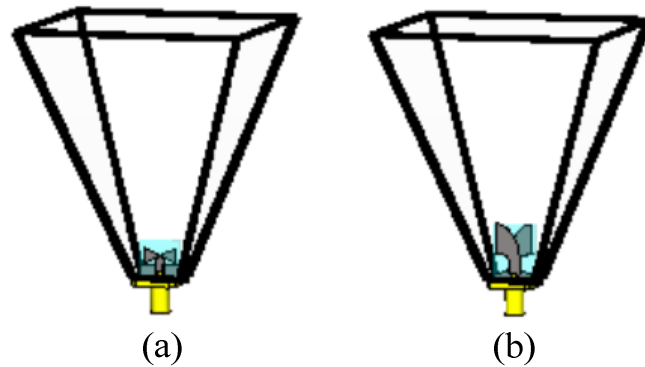


Figure 2.9 : Pyramidal horn antenna fed by planar antennas (Pítra and Raida, 2010):
(a) Bow-tie dipole; (b) Vivaldi

2.5.4 Pyramidal horn antenna excitation by microstrip antenna

Kumar et al. (Kumar et al., 2006) reported that new integrated configurations of pyramidal horn antenna excited by suspended square microstrip antenna (MSA). The method employed is similar with the one reported by Pitra and Raida (Pítra and Raida, 2010) where MSA is placed directly inside the pyramidal horn. The flexibility in the BW and the polarization were obtained with higher peak gain of 11 dBi as reported in (Kumar et al., 2006). It was found that the MSA structure governs the characteristics of the BW, polarization and radiation patterns. The BW of the pyramidal horn is 185 MHz (5.7%) centered at 3.3 GHz. However, the excitation configurations developed are for low frequency bands. The method of the proposed

excitation is shown in Figure 2.10 where the pyramidal horn antenna is constructed using suspended square MSA.

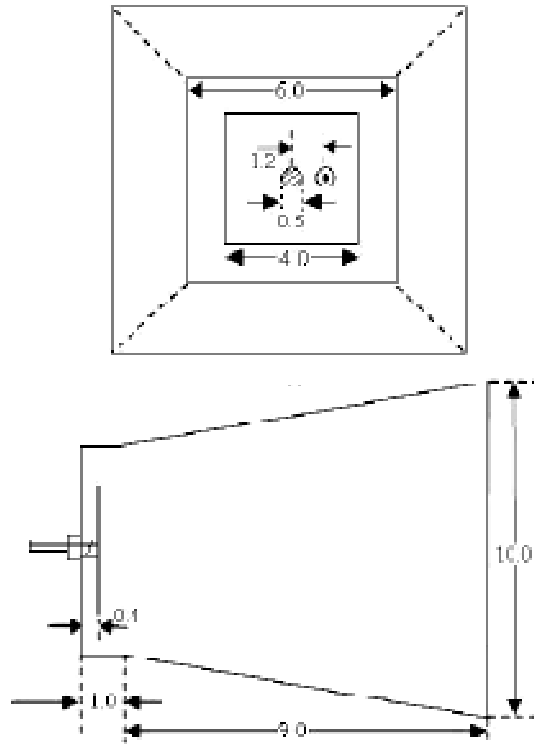


Figure 2.10 : Integrated suspended square MSA fed pyramidal horn antenna (unit : cm) (Kumar et al., 2006)

2.5.5 Pyramidal horn antenna excitation by microstrip patch

Recently, Ononchimeg et al.(Ononchimeg et al., 2011), have reported a new method of excitation for pyramidal horn antenna where microstrip patch is used in order to excite the pyramidal horn (Ononchimeg et al., 2011). A combination of the patch and horn is introduced for the center frequency of 14.9 GHz. The method is similar to the stacked patch pyramidal horn antenna reported by Shireen et al. The antenna gain of 12.34 dBi is achieved with 4.1% (600 MHz) impedance BW of -10 dB reflection. The structure of the proposed excitation method is shown in Figure 2.11. The